

UCLA

UCLA Previously Published Works

Title

Antigen presentation by clonally diverse CXCR5+ B cells to CD4 and CD8 T cells is associated with durable response to immune checkpoint inhibitors

Permalink

<https://escholarship.org/uc/item/55f9w4qm>

Authors

Ding, Lizhong

Sun, Lu

Bu, Melissa T

et al.

Publication Date

2023

DOI

10.3389/fimmu.2023.1176994

Peer reviewed



OPEN ACCESS

EDITED BY

Hui Zhao,
University of Texas MD Anderson Cancer
Center, United States

REVIEWED BY

Hunter Shain,
University of California, San Francisco,
United States
Ali Roghanian,
University of Southampton,
United Kingdom

*CORRESPONDENCE

Melissa G. Lechner
✉ mlechner@mednet.ucla.edu
Willy Hugo
✉ whilly@mednet.ucla.edu

RECEIVED 01 March 2023

ACCEPTED 22 May 2023

PUBLISHED 26 June 2023

CITATION

Ding L, Sun L, Bu MT, Zhang Y, Scott LN,
Prins RM, Su MA, Lechner MG and Hugo W
(2023) Antigen presentation by clonally
diverse CXCR5+ B cells to CD4 and CD8 T
cells is associated with durable response to
immune checkpoint inhibitors.
Front. Immunol. 14:1176994.
doi: 10.3389/fimmu.2023.1176994

COPYRIGHT

© 2023 Ding, Sun, Bu, Zhang, Scott, Prins,
Su, Lechner and Hugo. This is an open-
access article distributed under the terms of
the [Creative Commons Attribution License
\(CC BY\)](https://creativecommons.org/licenses/by/4.0/). The use, distribution or
reproduction in other forums is permitted,
provided the original author(s) and the
copyright owner(s) are credited and that
the original publication in this journal is
cited, in accordance with accepted
academic practice. No use, distribution or
reproduction is permitted which does not
comply with these terms.

Antigen presentation by clonally diverse CXCR5+ B cells to CD4 and CD8 T cells is associated with durable response to immune checkpoint inhibitors

Lizhong Ding^{1,2}, Lu Sun^{2,3}, Melissa T. Bu¹, Yanjun Zhang^{1,4},
Lauren N. Scott⁵, Robert M. Prins^{2,3,6,7}, Maureen A. Su^{2,7,8,9},
Melissa G. Lechner^{5,8*} and Willy Hugo^{1,2,8*}

¹Department of Medicine, Division of Dermatology, University of California, Los Angeles, Los Angeles, CA, United States, ²Parker Institute for Cancer Immunotherapy, University of California, Los Angeles, Los Angeles, CA, United States, ³Department of Neurosurgery, University of California, Los Angeles, Los Angeles, CA, United States, ⁴State Key Laboratory of Experimental Hematology, Institute of Hematology and Blood Diseases Hospital, Chinese Academy of Medical Sciences and Peking Union Medical College, Beijing, China, ⁵Department of Medicine, Division of Endocrinology, Diabetes, and Metabolism, University of California, Los Angeles, Los Angeles, CA, United States, ⁶Department of Molecular and Medical Pharmacology, University of California, Los Angeles, Los Angeles, CA, United States, ⁷Jonsson Comprehensive Cancer Center, University of California, Los Angeles, Los Angeles, CA, United States, ⁸Department of Microbiology, Immunology, and Molecular Genetics, University of California, Los Angeles, Los Angeles, CA, United States, ⁹Department of Pediatrics, Division of Pediatric Endocrinology, University of California, Los Angeles, Los Angeles, CA, United States

Introduction: Increased T cell infiltration and interferon gamma (IFN γ) pathway activation are seen in tumors of melanoma patients who respond to ICI (immune checkpoint inhibitor) or MAPK pathway inhibitor (MAPKi) therapies. Yet, the rate of durable tumor control after ICI is almost twice that of MAPKi, suggesting that additional mechanisms may be present in patients responding to ICI therapy that are beneficial for anti-tumor immunity.

Methods: We used transcriptional analysis and clinical outcomes from patients treated with ICI or MAPKi therapies to delineate immune mechanisms driving tumor response.

Results: We discovered response to ICI is associated with CXCL13-driven recruitment of CXCR5+ B cells with significantly higher clonal diversity than MAPKi. Our *in vitro* data indicate that CXCL13 production was increased in human peripheral blood mononuclear cells by anti-PD1, but not MAPKi, treatment. Higher B cell infiltration and B cell receptor (BCR) diversity allows presentation of diverse tumor antigens by B cells, resulting in activation of follicular helper CD4 T cells (Tfh) and tumor reactive CD8 T cells after ICI therapy. Higher BCR diversity and IFN γ pathway score post-ICI are associated with significantly longer patient survival compared to those with either one or none.

Conclusions: Response to ICI, but not to MAPKi, depends on the recruitment of CXCR5+ B cells into the tumor microenvironment and their productive tumor antigen presentation to follicular helper and cytotoxic, tumor reactive T cells. Our study highlights the potential of CXCL13 and B cell based strategies to enhance the rate of durable response in melanoma patients treated with ICI.

KEYWORDS

melanoma, immunotherapy, checkpoint inhibitors, interferon gamma pathway, tertiary lymphoid structure (TLS), T cell, B cell, antigen presentation

Introduction

Metastatic melanoma used to have a dismal median overall survival of only nine months after diagnosis (1, 2). However, the advent of immune and targeted therapies (3, 4) has significantly improved the survival of patients with metastatic melanoma. The highly immunogenic nature of melanoma has made it the model cancer to study response to immune checkpoint inhibitors (ICI), such as the blocking antibodies against T cell inhibitory receptors (T cell “checkpoints”) such as cytotoxic T lymphocyte antigen (CTLA)-4 and programmed death protein (PD)-1 (5–8). Despite the remarkable success of ICIs in many patients with melanoma, their clinical response remains difficult to predict (9–12). Previous work highlighted the association of T cell infiltration and patient response to ICI; ICI-treated tumors displayed a higher number of infiltrating T cells accompanied by expression of genes related to interferon pathway activities, demonstrating increased production of interferon gamma (IFN γ) of these T cells (13–17).

The discovery of constitutive activation of RAF/MEK/ERK signaling *via* the BRAF V600 mutation in nearly half of all cutaneous melanoma cases also revolutionized cancer therapy (18). MAPK pathway inhibitor (MAPKi) treatment significantly prolonged the survival of metastatic melanoma patients with BRAF V600 mutation (BRAF^{V600} mutant melanoma) (19–21). In addition to its direct tumor suppressive effect through MAPK pathway inhibition, MAPKi treatment also increases the infiltration of antitumor T cells into the tumor microenvironment (TME), suggesting immune modulatory effects (22, 23).

Intriguingly, despite MAPKi therapy having a higher rate of initial response than ICI (MAPKi (dabrafenib+ trametinib): 67% (19), MAPKi (vemurafenib+cobimetinib): 68% (20) vs ICI (nivolumab and ipilimumab): 58% (8)), the 5-year survival rate of BRAF^{V600} mutant subset of melanoma patients treated with MAPKi is only around half that of ICI (34% using dabrafenib and trametinib (24), 31% using vemurafenib and cobimetinib (25) vs. 60% after nivolumab and ipilimumab (26)). Furthermore, a matching-adjusted study found that ICI treatment improved overall survival (OS) of BRAF-mutant melanoma patients when compared to MAPKi (27). While acknowledging some differences among these studies, this consistent and significant difference in durable survival between ICI and MAPKi treated melanoma

patients suggests that there may be fundamental differences in the anti-tumor responses induced by these therapies.

To discover such differences, this study analyzes the changes in immune related gene expressions that are significantly associated with survival of melanoma patients after ICI or MAPKi treatment. Previous work compared on-treatment tumors (i.e., these tumor samples were biopsied after treatment) of patients responding to ICI (ICI OT-R) compared with those from patients not responding to ICI (ICI OT-NR) to nominate immune factors/pathways associated with response to ICI (15–17). However, this comparison is not necessarily informative. Since ICI OT-NR tumors generally have less immune infiltration compared to ICI OT-R, most immune cell-related markers will be upregulated in ICI OT-R group. Which of these are drivers of ICI's durable response vs. insignificant bystanders is therefore unclear. Since MAPKi OT-R tumors also have more immune infiltration than MAPKi OT-NR tumors, yet MAPKi OT-R patients are less likely to achieve a durable response than ICI OT-R patients, we posit that immune genes/pathways that are upregulated/enriched in ICI OT-R, but not in MAPKi OT-R tumors, can help explain the higher rate of durable responses in ICI treated patients.

In this report, we used transcriptional analysis and clinical outcomes from patients treated with ICI or MAPKi therapies to delineate immune mechanisms driving tumor response. We discovered higher expression of genes related to B cell recruitment in the ICI OT-R tumor, such as the ligand/receptor pair *CXCL13* and *CXCR5*. Anti-PD1 antibody treatment of human immune cells upregulated *CXCL13* while MAPKi inhibited *CXCL13* production, suggesting that differential regulation of *CXCL13* by these two treatments may dictate treatment outcomes. Single cell RNA-seq analysis of ICI-treated melanoma confirmed that response to ICI increased the number of germinal center-like B cells and its associated T follicular helper CD4 T cells, indicative of tertiary lymphoid structure (TLS) formation as reported previously (28–31). These cells were recruited into the TME by *CXCL13*-producing, cytotoxic CD8 T cell population that was specific to ICI. Importantly, BCR diversity, but not clonality, was significantly associated with extended overall survival after ICI but not MAPKi. The significant association between BCR diversity and survival after ICI suggests that ICI-induced B cells serve as antigen presenting cells, which will be able to cover more tumor

antigens with more diversified BCR clones. Indeed, patients whose tumors display both higher BCR diversity and IFN γ signaling pathway scores after ICI, which suggest successful antigen presentation by B cells to T cells, have significantly longer overall survival than those with either one or none. Our results suggest a combination of ICI with therapies that enhance immigration of and antigen presentation by clonally diverse B cells can result in a more durable antitumor immune response.

Materials and methods

Datasets used

In order to perform a comparative analysis on transcriptomic response to ICI and MAPKi, we analyzed two batches of immunotherapy data and two batches of targeted therapy data. The two immunotherapy datasets are from Riaz N, et al. (32) (named 2017_Cell_NR) and Abril-Rodriguez G, et al. (16) (named 2020_NC_GA). The patients from the two cohorts were treated with antibodies against PD-1 receptor (anti-PD-1) including nivolumab and pembrolizumab. The two targeted therapy datasets are derived from Hugo W, et al. (23, 33) (named 2015_Cell_WH) and from Kwong LN, et al. (34) (named 2015_JCI_LK). Two microarray datasets of MAPKi-treated tumors were used as validation cohort (35, 36). Patients in the targeted therapy datasets were treated with either BRAF inhibitor monotherapy or BRAF and MEK inhibitors combination therapy (BRAFi: vemurafenib, dabrafenib, encorafenib; MEKi: cobimetinib, trametinib, binimetinib; one patient was treated with trametinib monotherapy). All samples were classified into three groups: pre-treatment (PT), on-treatment responding (OT-R), and on-treatment non-responding (OT-NR). OT-R is defined by clinical benefit after therapy (CR, PR, or SD by RECIST criteria). OT-NR is defined by no clinical benefit (PD) (Supp. Table 1A). For single cell transcriptome analysis, we utilized the data from Sade-Feldman et al. (37). The data profiled 16,291 immune cells (CD45+ cells) from 48 tumor samples of melanoma patients treated with ICI. All samples were classified into four groups: pre-treatment responding (PT-R), pre-treatment non-responding (PT-NR), on-treatment responding (OT-R), and on-treatment non-responding (OT-NR). The PFS and OS data of MAPKi treated patients were extracted from the above-mentioned two microarray datasets (Supp. Table 2).

The bulk RNA-seq data were downloaded from the following online repositories. 2017_Cell_NR (ICI) was from PRJNA356761; 2020_NC_GA (ICI) was from PRJNA578193; 2015_Cell_WH (MAPKi) was from PRJNA273359, PRJNA303170, PRJNA403850; 2015_JCI_LK (MAPKi) was from EGAD00001001306. The single cell RNA-seq data were downloaded from the GEO database (accession ID: GSE120575). Instead of the TPM normalized expression values, we started from the raw counts provided by the authors in personal communications. The raw count expression values were included in the source code of this study. Two microarray data sets of MAPKi-treated melanoma were downloaded from GEO (accession ID: GSE61992 and GSE50509).

Gene expression analysis

The bulk RNA-seq data was re-aligned to hg38 human reference genome using HiSAT2 (v2.1.0), then processed using samtools (v1.10, RRID : SCR_002105) and picard (v2.25.0). The gene expression count was calculated using htseq-count (v0.11.2). The gene expression was normalized using trimmed mean of M-values (TMM) and converted to count per million (cpm) expression value using the R package edgeR (v3.32.1, RRID : SCR_012802). Batch effect was corrected using removeBatchEffect function in the R package limma (v3.46.0).

Differential gene expression analysis

We first computed the expression change of each gene (in log₂ FC) between the PT and OT samples of each patient (the OT samples can be OT-R or OT-NR). Thus, each gene will have a list of log₂ FC values associated with therapy response (OT-R with respect to their respective PT) and resistance/non-response (OT-NR w.r.t their respective PT) (Figure 1A). Differentially expressed genes (DEGs) between the OT-R and OT-NR groups were defined by:

1. two-fold difference between the arithmetic average of log₂ FCs in OT-R and arithmetic average of log₂ FCs in OT-NR ($\Delta\log_2 \text{FC} \geq 1$ where $\Delta\log_2 \text{FC} = \text{mean}(\log_2 \text{FC}(\text{OT-R})) - \text{mean}(\log_2 \text{FC}(\text{OT-NR}))$), and,
2. FDR-adjusted t-test p value < 0.05 between the log₂ FCs of the OT-R and OT-NR groups.

The sets of DEGs upregulated in the OT-R groups of either therapy were shown in Figure 1B. The gene sets/ontologies that are enriched in the ICI-specific, MAPKi-specific and ICI and MAPKi shared DEGs were computed using Enrichr (38) (see the **gene set analysis** section). Other than comparing the list of DEGs, we also directly computed the difference of log₂ FC difference between the OT-R and OT-NR groups across the two therapies. For instance, to find the genes that are upregulated at least two-fold higher in ICI's responder when compared to MAPKi responders (after adjusting with their respective non-responder groups), we selected genes satisfying:

1. $\Delta\Delta\text{FC}_{\text{ICI-MAPKi}} \geq 1$, where $\Delta\Delta\text{FC}_{\text{ICI-MAPKi}} = \Delta\log_2 \text{FC}_{\text{ICI}} - \Delta\log_2 \text{FC}_{\text{MAPKi}}$, and,
2. $\Delta\log_2 \text{FC}_{\text{ICI}} \geq 1$

Conversely, the genes upregulated in MAPKi's responders were computed in the same manner.

Gene sets analysis

Shortlisted genes from DEG analysis were analyzed for overlap-based gene set enrichment using Enrichr (38). Top enriched gene sets from Human_Gene_Atlas and HuBMAP_ASCT_plus_B_

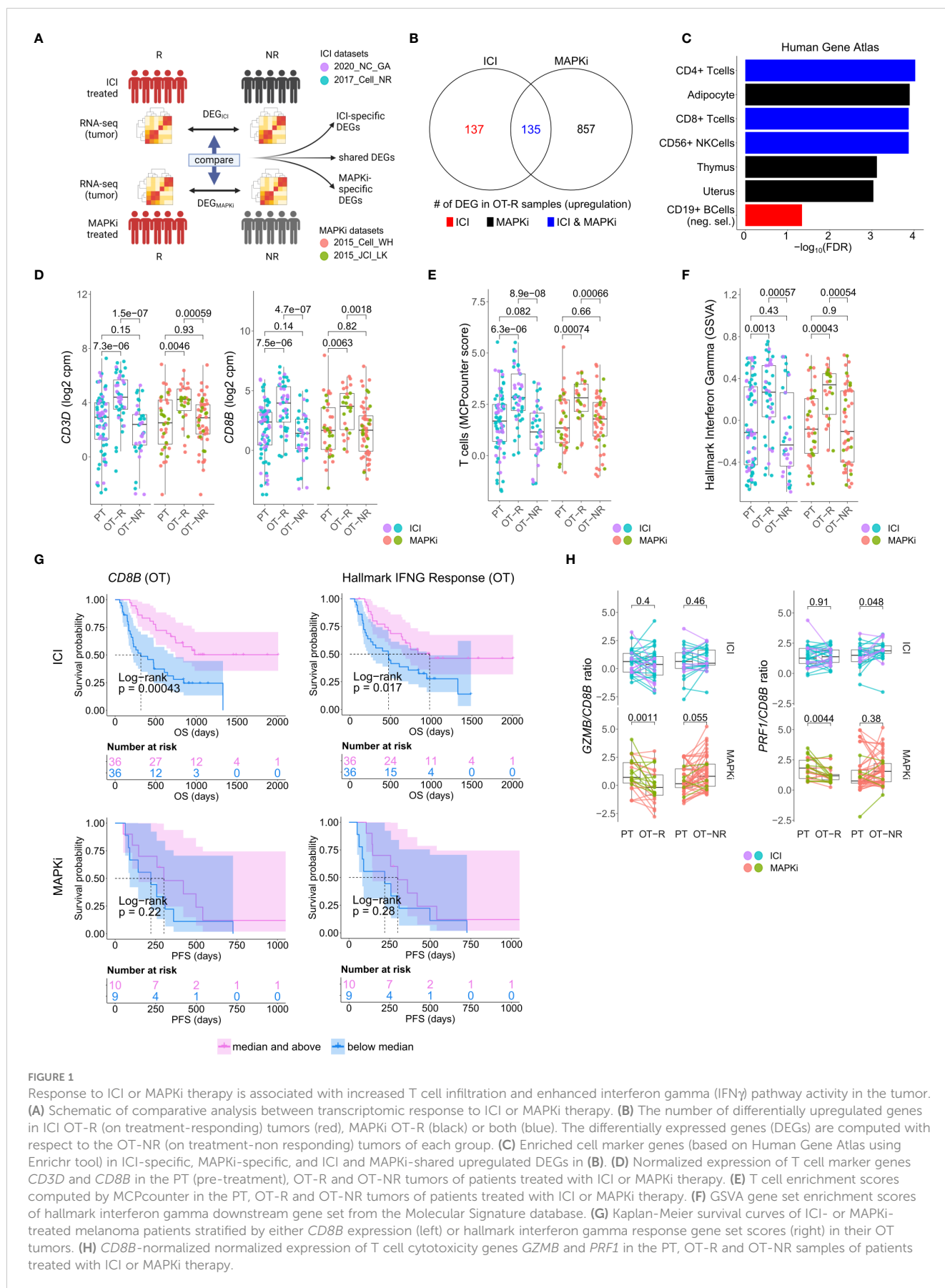


FIGURE 1

Response to ICI or MAPKi therapy is associated with increased T cell infiltration and enhanced interferon gamma (IFN γ) pathway activity in the tumor. (A) Schematic of comparative analysis between transcriptomic response to ICI or MAPKi therapy. (B) The number of differentially upregulated genes in ICI OT-R (on treatment-responding) tumors (red), MAPKi OT-R (black) or both (blue). The differentially expressed genes (DEGs) are computed with respect to the OT-NR (on treatment-non responding) tumors of each group. (C) Enriched cell marker genes (based on Human Gene Atlas using Enrichr tool) in ICI-specific, MAPKi-specific, and ICI and MAPKi-shared upregulated DEGs in (B). (D) Normalized expression of T cell marker genes *CD3D* and *CD8B* in the PT (pre-treatment), OT-R and OT-NR tumors of patients treated with ICI or MAPKi therapy. (E) T cell enrichment scores computed by MCPcounter in the PT, OT-R and OT-NR tumors of patients treated with ICI or MAPKi therapy. (F) GSEA gene set enrichment scores of hallmark interferon gamma downstream gene set from the Molecular Signature database. (G) Kaplan-Meier survival curves of ICI- or MAPKi-treated melanoma patients stratified by either *CD8B* expression (left) or hallmark interferon gamma response gene set scores (right) in their OT tumors. (H) *CD8B*-normalized normalized expression of T cell cytotoxicity genes *GZMB* and *PRF1* in the PT, OT-R and OT-NR samples of patients treated with ICI or MAPKi therapy.

augmented_w_RNAseq_Coexpression collections are visualized in [Figure 1C](#) and listed in [Supp. Table 1C](#). Score based, single sample gene set enrichments was computed using Gene Set Variation Analysis (GSVA) (39) through R packages GSVA (v1.38.2), GSVAdat (v1.26.0), and GSEABase (v1.52.1).

We used the interferon gene sets from the Molecular Signatures Database (MSigDB) (40, 41). Specifically, we collected gene sets containing the keyword “IFN” or “interferon” from the H: hallmark gene sets, C2 CGP: chemical and genetic perturbations, C6: oncogenic signatures, and C7: immunologic signatures ([Supp. Table 1E](#)). The gene set of TLS signatures were manually curated in gmt file format. Cabrita et al. developed two gene sets that reflected the presence of TLS in melanoma. One TLS signature of nine genes (*CD79B*, *CD1D*, *CCR6*, *LAT*, *SKAP1*, *CETP*, *EIF1AY*, *RBP5*, *PTGDS*) was found using differential expression analysis. The other TLS signature of seven genes (*CCL19*, *CCL21*, *CXCL13*, *CCR7*, *CXCR5*, *SELL*, *LAMP3*) was constructed from a compendium of TLS hallmark genes (29).

Clonotype analysis

As for the TCR clonotyping, the raw output of clonotypes was derived from the raw FASTQ reads of the bulk RNA-seq data using TRUST4 (v1.0.4) (42) with default settings. Nonproductive CDR3aa were removed from the raw output. Clonotypes are separated by chain names such as TRA, TRB, TRD, TRG, IGH, IGK, IGL. Convergent clonotypes, which possess the same amino acid sequences but different nucleotide sequences, were merged. As for the BCR clonotyping, considering the somatic hypermutation (SHM) mechanism of germinal center (GC) B cells, productive IGH chains were selected from the raw AIRR standard format output derived from the bulk RNA-seq data using TRUST4 (v1.0.4). Then the hierarchicalClones() function in the R package SCOPer (43) (v1.2.0) was used to infer—based on the nucleotide sequence—the germline BCR clones that arise from V(D)J recombination (in the bone marrow) and mature (SHM-generated) BCR clones that are derived from germline BCR clones after somatic hypermutation process in the germinal center (44). The R package SHazaM (45) (v1.1.0) was used to automatically calculate the threshold for the bimodal distribution from the hierarchicalClones() function as defined by the SCOPer pipeline. Consequently, the SHM occurrence frequency can be calculated using the count of germline BCR clones associated with more than one mature BCR clone divided by total count of the germline BCR clones. The clonotype repertoire metrics of TCR and BCR, including count, diversity, and clonality were calculated using the custom R package rTCRBCRr (v0.1.0) and other custom R scripts.

Cell population abundance estimation

The R package MCPcounter (v1.2.0) was applied to the normalized log₂ cpm expression matrix from the bulk RNA-seq data in order to estimate the absolute abundance of eight immune and two stromal cell populations in each sample, including T cells,

CD8 T cells, cytotoxic lymphocytes, B lineage, NK cells, monocytic lineage, myeloid dendritic cells, neutrophils, endothelial cells, and fibroblasts ([Supp. Table 1D](#)).

Overlap-based gene set enrichment

The enrichment of specific biological process or gene ontologies were analyzed using Enrichr, which is implemented in enrichR R package (v3.0) (38). Specifically, lists of DEGs were tested for significant overlaps with pre-curated gene sets within the Enrichr based on fisher exact test. The P values we utilized were the ones adjusted for multiple tests using the FDR method and the cutoff of enriched gene set term is adjusted P value < 0.05.

Survival analysis

The Kaplan-Meier curves were used to visualize differences in survival between patient groups. Cox proportional hazard (Cox PH) regression was used to assess the effect of single or multiple variables on hazard ratio. These analyses were performed using the R packages survival (v3.2.13) and visualized using survminer (v0.4.9), and survivalAnalysis (v0.3.0). For PFS analysis in the MAPKi-treated cohort, we only included OT tumors biopsied prior to progression (giving a total 25 OT tumors from 19 MAPKi-treated patients).

Single cell analysis

The single cell data was processed using the R package Seurat (v4.0.2). The raw count data were provided by the authors. We first normalized the raw counts using the NormalizeData() function with normalization.method=“LogNormalize” and scale.factor=10000. 17 clusters were identified at resolution=0.5. Cell types of the clusters were manually annotated based on each cluster’s gene markers, which were computed using FindAllMarkers() (min.pct=0.25 and logfc.threshold=0.585). The R package AUCell (v1.12.0) was used to identify gene set enrichments in the single cell transcriptome. The R package CellChat (v1.1.3) was used to visualize cell-cell communication network, grouped by different signaling pathways, among different cell types.

Statistical analysis

All the statistical analysis were performed using R programming language version 4.0.5. Unless otherwise stated, all the statistical tests were two tailed. In all boxplots, including gene expression, GSVA score, and gene expression ratio, P values were calculated using a two-sided Wilcoxon rank sum test. In all boxplots, the median is indicated by the line within the box and the 25th and 75th percentiles indicated by the lower and upper bounds of the box. The upper and lower lines above and below the boxes represent the whiskers. Pearson’s R correlation coefficient was computed using

R's *cor.test* function. The P values of the Pearson's R correlation coefficient were computed using two-sided t-test as described in the documentation. In the Kaplan-Meier survival curves, the P value is the log-rank test P value. In the Cox PH analysis, the P value shown for each variable in the graph is the result of Wald test.

In vitro assessment of primary human immune cells

Peripheral blood mononuclear cells (PBMC) from healthy donors were isolated from blood by density gradient centrifugation (Ficoll-Hypaque). PBMC were cultured at 10^6 cells/well in 12 well plates in complete media with 2ME. Stimulation was provided by anti-CD3/CD28 Dynabeads (Invitrogen), as well as anti-human PD-1 (clone pembrolizumab, BioXcell, RRID: AB_2894731), MEKi trametinib (LSBiosciences) and BRAFi dabrafenib (BioVision), or vehicle. Supernatants were collected on day 5. Secreted CXCL13 was quantified in supernatants by ELISA (R&D Systems). The concentrations chosen for dabrafenib and trametinib was based on reported maximum plasma concentration in patients, which were 2.4 μ M and 0.03 μ M, respectively (46). To avoid overactivation of the T cells in the PBMC, we chose a lower PD-1 antibody concentrations (1 and 10 μ g/mL) than the median C_{max} and C_{trough} of pembrolizumab (89.1 and 27.6 μ g/mL) (47).

Results

ICI and MAPKi treatment induce comparable levels of T cell infiltration

To perform a comparative analysis of transcriptomic response to ICI and MAPKi, we analyzed three separate immunotherapy datasets (16, 32, 37) and three targeted therapy datasets (23, 33, 34) (Supp. Figure 1A; Supp. Table 1A). All samples were classified into three groups: pre-treatment (PT), on-treatment responding (OT-R), and on-treatment non-responding (OT-NR). OT-R is defined by clinical benefit after therapy (CR, PR, or SD by RECIST criteria). OT-NR is defined by no clinical benefit (PD) (Supp. Table 1A). Gene expression in samples across the datasets were integrated and batch normalized (see Methods).

We asked whether the set of differentially expressed genes (DEG) between ICI and MAPKi could reveal any cell populations or biological processes that may explain ICI's more durable antitumor response. To this end, we selected genes upregulated in the OT-R compared to the OT-NR samples for each therapy (Figure 1A, see Methods for details). The upregulated DEG were grouped into either ICI-specific, MAPKi-specific, or ICI and MAPKi-shared (Figure 1B; Supp. Table 1B), and gene sets enriched by these DEGs were computed using Enrichr (38). We first noted gene sets related to T cells being enriched in the OT-R groups of both therapies (Figure 1C; Supp. Tables 1C, D). Indeed,

increased T cell infiltration and activity are important for both ICI and MAPKi response (13, 15, 17, 22, 32, 37, 48) and the levels of general T cell marker (*CD3D*), cytotoxic CD8 T cells (*CD8B*), T cell signature and IFN γ pathway score were significantly higher in the OT-R tumors of MAPKi or ICI compared to PT and OT-NR tumors (Figures 1D–F; Supp. Tables 1D, E). T cell marker expressions and IFN γ pathway score were not significantly different between ICI and MAPKi in either PT, OT-R or OT-NR samples (Supp. Figures 1B, C). Our data suggests that response to ICI or MAPKi induces a robust increase in T cell infiltration and IFN γ pathway activation in the TME.

Intriguingly, only higher normalized expression of CD8 T cell marker *CD8B* or higher IFN γ gene set enrichment in ICI OT tumors, but not MAPKi OT tumors, was significantly correlated with longer survival (Figure 1G). Neither *CD8B* expression nor IFN γ pathway score in PT biopsies was significantly correlated with survival (Supp. Figure 1D), indicating the importance of T cell infiltration and activity after therapy. Using a separate microarray dataset of MAPKi OT tumors (35, 36), we confirmed that neither higher *CD8B* nor higher IFN γ gene set enrichment was correlated with OS and PFS after MAPKi therapy (Supp. Figure 1E). Since the MAPKi RNA-seq datasets only have progression free survival (PFS) information available and since melanoma patients' PFS is significantly correlated with their OS in the MAPKi microarray data (Supp. Figure 1F), we will use PFS differences in the MAPKi cohort as a surrogate of OS differences in later analysis of the MAPKi RNA-seq datasets.

We noted higher total expression of T cell cytotoxicity-related genes, *GZMB* and *PRF1*, in ICI OT-R than MAPKi OT-R (Supp. Figure 1G). We further estimated the levels of these cytotoxicity-related genes on a per T cell basis by computing the ratio between normalized expression of the markers and *CD8B*. On this approximated per-CD8 basis, MAPKi-treated responders had lower *GZMB* and *PRF1* expression than their patient-matched PT tumors while ICI-treated responders did not show such a decrease (Figure 1H). Overall, our analysis demonstrated that ICI treatment induces the infiltration of more cytotoxic CD8 T cells into the TME compared to MAPKi and such increase in T cell activity is significantly correlated with patient OS after ICI therapy.

B cells are more abundant in ICI On Treatment Responding tumors and are correlated with improved survival after ICI therapy

We next examined ICI-specific DEGs to discover additional cell populations or pathways that are significantly associated with response to ICI therapy. On one hand, genes related to B cells and DC gene sets (Figures 1C; 2A; Supp. Table 1C) were upregulated in ICI OT-R tumors compared to MAPKi OT-R tumors (after adjusting against the average expression of the same genes in the respective OT-NR groups, see Methods). On the other

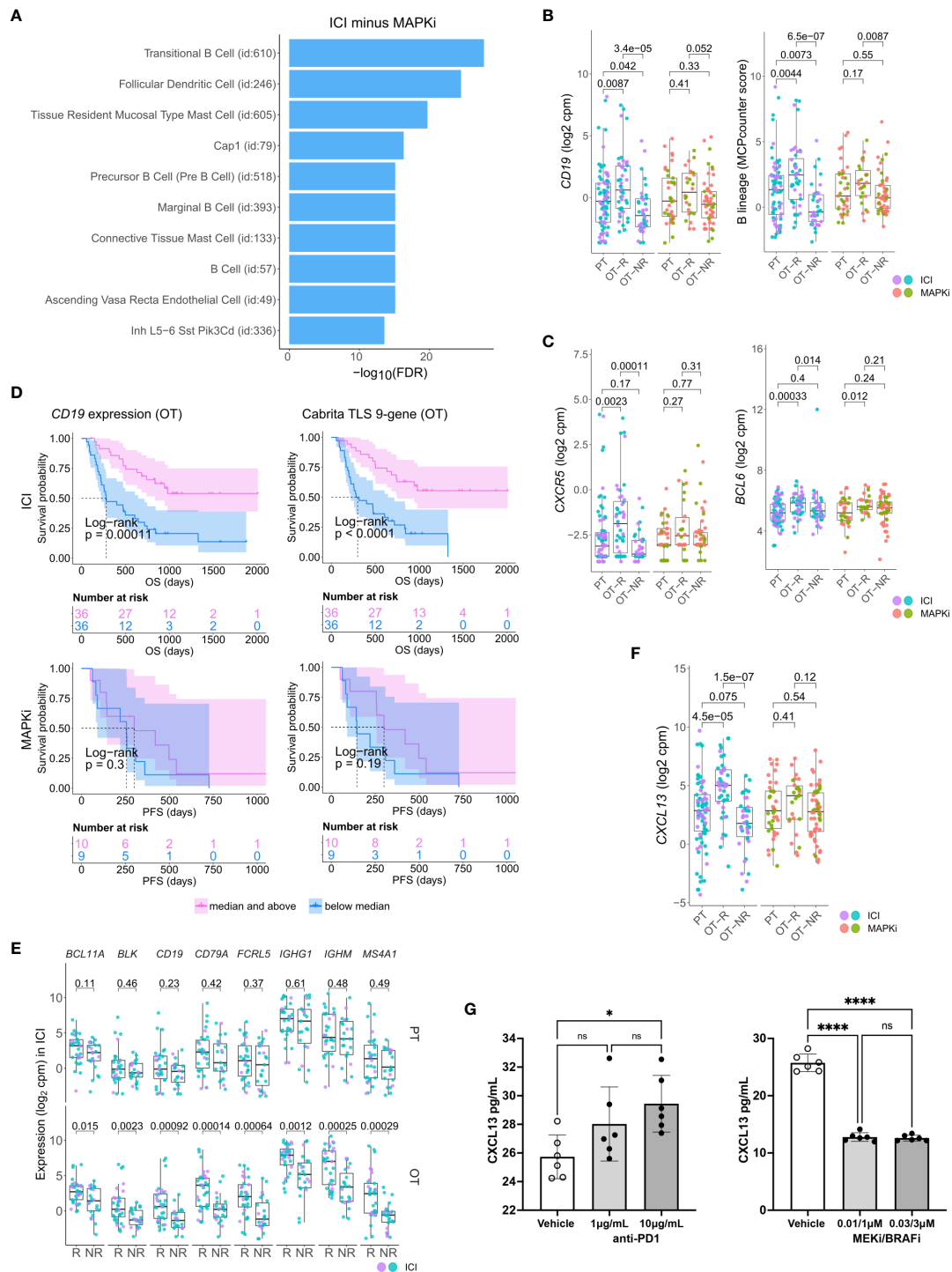


FIGURE 2

Relative increase of B cell and tertiary lymphoid structure (TLS) marker genes in response to ICI therapy compared to MAPKi. (A) Enriched tissue specific gene sets in DEGs upregulated in ICI OT-R tumors with respect to MAPKi OT-R tumors (after adjustment by respective therapy group's OT-NR tumors; see Methods). (B) Normalized expression of B cell marker genes and enrichment of B cell lineage gene set among the PT, OT-R and OT-NR tumors in the ICI or MAPKi therapy group. (C) Normalized expression of TLS-related genes, *CXCR5* and *BCL6*, among the PT, OT-R and OT-NR tumors in the ICI or MAPKi therapy group. (D) Kaplan-Meier survival curves of ICI- or MAPKi-treated melanoma patients stratified by either *CD19* expression (left) or TLS gene set enrichment score (right) of their OT tumors. (E) Pairwise expression comparison of the listed B cell-related genes between PT (top) or OT (bottom) samples of melanoma patients stratified by response (R) or no response (NR) to ICI. (F) Normalized expression of *CXCL13* among the PT, OT-R and OT-NR tumors in the ICI or MAPKi therapy group. (G) *CXCL13* secretion by human peripheral blood mononuclear cells is increased by anti-PD-1 antibody treatment but decreased by trametinib (MEK inhibitor) + dabrafenib (BRAF V600E inhibitor) *in vitro*. The six points in each bar graph across represent the same PBMC samples from six donors; these were treated with the indicated amount of antibody/inhibitor or vehicle. Significance of pairwise comparisons was computed using t-test, * $p < 0.05$, **** $p < 0.0001$, ns, not significant.

hand, MAPKi OT-R tumors showed enrichment of non-immune related gene sets such as neuron, melanocyte and adipocyte related genes (Supp. Figure 2A; Supp. Table 1C).

There were more prominent upregulations of B cell gene markers, B cell signature and immunoglobulin genes in OT-R tumors, with respect to either OT-NR or PT tumors after ICI compared to MAPKi therapy (Figure 2B; Supp. Figure 2B; Supp. Tables 1C, D). Importantly, the expression of TLS-associated, germinal center B cell (GC B cells) and follicular helper T cell (Tfh) markers, *CXCR5* and *BCL6*, were significantly upregulated only in response to ICI but not MAPKi (Figure 2C). The presence of TLS has been correlated with improved survival after ICI therapy in melanoma (28, 29) and other cancers (30, 31). ICI treatment also induced a more significant increase of gene set scores of two TLS signatures (29) compared to MAPKi (Supp. Figure 2C; Supp. Table 1E). The magnitude of *CD19* expression and TLS signature score both significantly correlated with survival after ICI but not MAPKi therapy (Figure 2D; Supp. Figure 2D). On the other hand, the level of B cell marker or the TLS signature in the PT samples is not associated with survival after ICI treatment (Supp. Figure 2E). In agreement with the survival data, B cell marker expression was positively correlated with tumor response to ICI in OT but not PT tumors (Figure 2E), suggesting that the expression of B cell and TLS marker genes pre-therapy are relatively weak predictors of ICI response and survival in melanoma patients.

Among ICI-specific differentially expressed of cytokines and chemokines was *CXCL13*, which is the ligand for *CXCR5* and a key chemokine for the formation of TLS (Figure 2F). The upregulation of *CXCL13* after ICI treatment is expected to recruit *CXCR5*+ B cells and *CXCR5*+ Tfh cells. We tested if ICI can directly increase *CXCL13* expression in human immune cells. Incubation of anti-CD3/28 activated peripheral blood mononuclear cells (PBMC) with anti-PD-1 antibody increased the secretion of *CXCL13* protein (Figure 2G, left). In contrast, treatment with BRAF and MEK inhibitors (MAPKi) significantly inhibited *CXCL13* secretion (Figure 2G, right). Thus, *CXCL13* production is promoted by anti-PD1 antibody, but impaired by BRAF and MEK inhibitors. The increase in *CXCL13* was associated with increased expression of B cell and TLS-associated markers (*CXCR5*, *BCL6*) in ICI OT-R tumors.

Enrichment of B cell and Tertiary Lymphoid Structure gene markers in single cell transcriptome of ICI responding melanoma

To analyze potential connections between enhanced CD8 T cell cytotoxicity and increased presence of TLS-associated B cells in ICI OT-R tumors, we examined single cell transcriptomic data of tumors from an independent cohort of ICI-treated melanoma patients (37). Since this scRNA-seq is done on a sampling of sorted CD45+ cells, we can only compare the relative abundances of immune populations within the samples. Nonetheless, we were able to analyze significantly increased/decreased expression of gene markers within each immune population, allowing us to identify the cellular source of DEGs in the bulk RNA-seq analysis.

After normalization and scaling of the gene expression values (see Methods), we re-clustered the single cells and identified the cell types based on differentially upregulated immune gene markers in each cluster (Figures 3A–C; Supp. Table 3A). Clusters of known immune populations, such as memory T cell (*CD4/8+ CCR7+ TCF7+*), activated CD8 T cell (*IFNG+* or high in interferon downstream genes (ISGs)), activated/exhausted CD8 T cell (*PDCD1+ CTLA4+ TOX+*) with high expression of *CXCL13*, B cell (*CD19+ MS4A1+*), plasma cell (*SDC1+ IGHG/A+*), NK cell (*FCGR3A+ GNLY+*), Treg (*FOXP3+ CTLA4+*), monocyte/macrophage (Mφ) (*CD14+ CD163+*), monocyte-derived dendritic cells (monocytic DC: *CD14+ CLEC10A+*), plasmacytoid DC (*LILRA4+*) and proliferating immune cell (*MKI67+*), were marked accordingly. We identified a *CXCR5+ BCL6+ CXCL13+* follicular helper T cell (Tfh) population in a subset of *PDCD1+ CXCL13+ CTLA4+ TOX+ TCF7+ CD4+* T cells (Figure 3B). We also noted the expression of *BCL6* and *REL* in the B cell population (Figure 3C); along with *BCL6*, *REL* is a transcription factor that is upregulated in GC B cells (44).

Corroborating the B cell marker up-expression in ICI OT-R tumors in bulk RNA-seq, we noted a significantly higher proportion of B cells in ICI OT-R samples compared to OT-NR samples (Figure 3D, red boxplots, bottom, Supp. Table 3B). We also noted that, in this scRNA-seq cohort, the proportion of B cells was already higher in the PT-R samples (Figure 3D, red boxplots, top, Supp. Table 3B). However, only B cell abundance in ICI OT tumors was significantly correlated with the patients' OS (Figure 3E; Supp. Table 3C).

Looking at the other cell populations, the proportion of *CCR7+ TCF7+* memory T cells per sample were higher in the PT-R and OT-R samples (Figure 3D, leftmost boxplot, Supp. Table 3B), in line with the original publication (37). Populations with a higher proportion in the OT-NR biopsies were the proliferating cluster and *CD14+ CD163+* Mφ clusters (Supp. Figure 3A; Supp. Table 3B). The proliferative cluster showed high expression of *CD3D*, *CD8A*, *PDCD1*, *CTLA4* and *TOX* (Figure 3B, rightmost boxplot); this population matches the phenotype of an intermediate exhausted cytotoxic T cells, which are expected to differentiate into terminally exhausted T cells (49). The *CD14+ CD163+* Mφ fraction was associated with worse OS after ICI (Supp. Figure 3B), suggesting that this is an immunosuppressive Mφ population.

In each cell population, we analyzed genes increased in expression in ICI OT-R tumors compared to OT-NR tumors (Supp. Table 3D). Consistent with evidence for GC B cells and Tfh in ICI-responders from the bulk RNA-seq cohort above, *CXCR5*+ B cells in OT-R showed increased expression of *BCL6* and *REL* (Figure 3F). We also confirmed that expression of *CXCR5* was significantly increased in Tfh/Tph population of ICI OT-R patients (Figure 3G, green boxplots), implying a higher proportion of Tfh cells in ICI OT-R tumors. The bulk RNA-seq cohorts showed an increased overall expression of *CXCL13*, which is the chemotactic factor for the *CXCR5*+ GC B and Tfh cells in ICI OT-R tumors. The scRNA-seq data allowed us to trace the source of *CXCL13* expression; *CXCL13* was significantly upregulated in the *PDCD1+ TOX+* CD8 T cell in ICI OT-R tumors (Figure 3G). Of note, *CXCL13+ PD1+ TOX+* CD8 T cell population was recently reported to comprise a high fraction of tumor antigen-specific CD8 T cells (50).

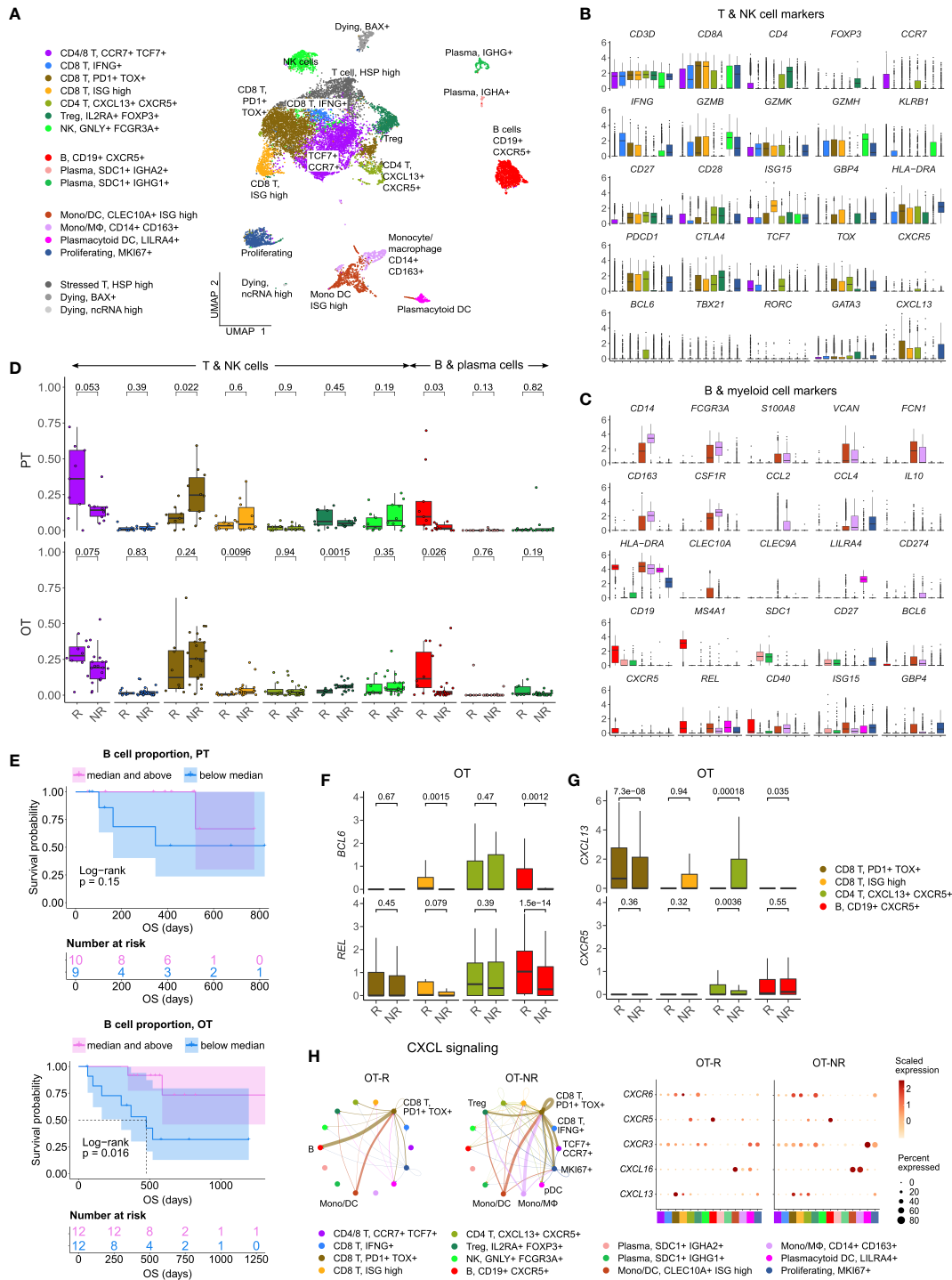


FIGURE 3

Increased B cell proportion is associated with TLS marker enrichments and improved OS in an independent cohort of ICI treated melanoma.

(A) UMAP projection of intratumoral CD45+ cells of ICI-treated melanoma. The cell type annotation of each cell cluster was inferred from the DEGs of each cluster. Mono/DC: monocytic DCs, Mono/Mφ: monocytes/macrophages. (B, C) Normalized expression of markers of cell type/activity among different T and NK cell (B) or B cell and myeloid cell populations (C). (D) The fraction of the T, NK, B and plasma cell populations in stratified by response vs. non-response to ICI in PT (top) and OT tumors (bottom). The boxplots are colored to match the cell clusters in (A). (E) Kaplan-Meier survival curves of ICI-treated patients stratified by the proportion of B cells within either their PT (top) or OT tumors (bottom). (F, G) Normalized expression of germinal center (GC) B cell markers, *BCL6* and *REL*, or follicular helper T cell (T_{fh}) markers, *CXCR5* and *CXCL13*, within the listed T/B cell populations from the scRNA-seq. (H) Predicted enrichment of receptor-ligand interaction involving the CXCL chemokine signaling in the ICI OT samples (left; the color of the connecting edge is the source cell's) and the normalized expression of the chemokine and their receptors in each immune population (right). The interaction involving the CXCL13-CXCR5 pair between tumor reactive *PDCD1+ TOX+* CD8 T cells and B cells was more enriched in ICI OT-R tumors.

CXCL chemokine-receptor interaction analysis using CellChat predicted that *CXCL13* expressed by *PD1+* *TOX+* CD8 T cells (source) mainly engaged CXCR5+ B cells (target) (Figure 3H, left). On the other hand, ICI OT-NR tumors show a mixture of CXCL16-CXCR6 and CXCL13-CXCR3 interaction among the monocytic DCs, macrophages and T cells (with weak CXCL13-CXCR5 interaction involving B cells). Although the relative fractions and normalized expression of *CXCL13* and *CXCR5* were similar between ICI OT-R and OT-NR (Figure 3H, dot plots), the CXCL13-CXCR5 interaction is expected to be stronger in ICI OT-R group since it has a larger fraction of CXCR5+ B cells among the CD45+ immune cells. Finally, AUCell analysis (51) showed enrichments of TLS gene sets specifically in B and Tfh cell clusters (Supp. Figure 3C), indicative of TLS formation within which CD8+ T, CD4+ Tfh and GC B cells interact with one another. Overall, our analyses illustrate ICI-mediated release of T cell checkpoint engagement of tumor-specific, PD1+ TOX+ CD8 T cells upregulates *CXCL13*, which subsequently recruits CXCR5+ B cells and Tfh to form TLS in the TME.

B cells and Tfh in ICI-responding tumors upregulate markers of productive antigen presentation

Using their B cell receptor (BCR), B cells can selectively capture antigens and present them to Tfh cells in through the MHC II antigen presentation pathway (52–54). For this interaction to happen, antigen-specific B cell clones must encounter cognate antigen-specific T cells in the T cell zones of the lymphoid follicle in secondary lymphoid organs or TLS. Indeed, our receptor-ligand interaction analysis suggests that intratumoral B cells in ICI OT-R tumors present antigens to CXCR5+ Tfh and Tregs through MHC II pathway (Figure 4A; Supp. Figure 4A). In OT-NR tumors, MHC II interaction was observed mostly between Tregs and multiple MHC II+ populations, including B cells, DC and the immunosuppressive Mφ (Figure 4A; Supp. Figure 4A).

Antigen recognition by Tfh results in the activation of their T helper function, providing stimulatory signal to CD40+ B cells through upregulation of CD40L (52). BCR ligation and CD40/CD40L pathway activation of B cells stimulates expression of APC maturation marker, *CD83*, which further strengthen the antigen presentation activity of B cells (55). Accordingly, we observed the upregulation of *CD40LG* and *CD83* transcripts in the Tfh and B cell populations, respectively (Figure 4B; Supp. Table 3D). Receptor-ligand interaction analysis on the genes in CD40 pathway also showed enrichment of the pathway only in ICI OT-R tumors (Figure 4C; Supp. Figure 4A). CD40L and IFN γ -induced activation can drive B cells to cross present antigens to CD8 T cells (56). Indeed, we confirmed that both CD40L and IFN γ pathways were active in the TME of ICI OT-R tumors and CellChat analysis predicted a significant MHC I pathway interaction between B cells and the tumor reactive *CXCL13+* *PD1+* *TOX+* CD8 T cells (Supp. Figure 4B).

Taken together, our single cell transcriptome analysis of ICI-treated melanoma demonstrated upregulation of gene markers and

enrichment of pathways associated with a productive antigen presentation by B cells to T cells in the TME of ICI OT-R tumors.

Diversity but not clonality of B cell population correlates with survival after ICI therapy

After a productive antigen presentation to T cells, antigen specific B cells can undergo class switch recombination (CSR), somatic hypermutation (SHM) and differentiation into long-lived plasma cells or memory B cells (52). It is unclear if ICI response in melanoma is associated with the formation of tumor-specific, antibody producing cells, as seen in clear cell renal cell carcinoma (31). We did not observe association between the relative abundances of plasma cells and response to ICI in the scRNA-seq cohort (Figure 3D). There were also very few cells expressing *CD19* or *MS4A1* within the *KI67+* proliferating cell cluster, indicating a rarity of proliferating B cells in this dataset (Figure 3C, based on the levels of the *CD19* or *MS4A1* in the rightmost proliferating cell cluster).

We applied TRUST4 to reconstruct the CDR3 regions within mRNA transcripts of immunoglobulin heavy (IGHA/M/G) chain in the bulk RNA-seq and scRNA-seq data (42). By defining each distinct IGH CDR3 sequence as a B cell clone, we can obtain an estimate of the B cells' clonal dynamics after ICI or MAPKi therapy. Response to ICI exhibited statistically significant increase of BCR diversity in ICI OT-R tumors (with respect to both PT and OT-NR) but not in MAPKi OT-R tumors (Figure 4D; Supp. Table 4A). SCOPer (43) analysis predicted an increased somatic hypermutation (SHM) in ICI OT-R tumors, which may have contributed to the increase of BCR diversity in ICI OT-R tumors (Figure 4E). We observed that most B cell clones in the ICI OT-R tumors were newly infiltrating clones after the therapy (Supp. Figure 4C). The same predominance of OT tumor specific clones can also be observed in the T cell populations (Supp. Figure 4D). The clonal dynamics of both T and B cells after ICI treatment matches the "T cell clonal replacement" event reported in basal/squamous cell carcinoma patients who responded to ICI (57).

Higher BCR diversity was associated with improved survival after ICI but not MAPKi therapy (Figure 4F). The significant correlation between BCR diversity and OS after ICI therapy was also confirmed in the scRNA-seq cohort (Figure 4G and Supp. Table 3E; Supp. Table 4B). BCR clonality was not associated with patient survival after ICI nor MAPKi therapy (Figures 4F, G). The observation of increased BCR diversity in response to ICI therapy suggests that B cells' role in the TME is to present T cells with a broad variety of tumor antigens. Since B cells present tumor antigens to T cells through BCR-specific internalization of extracellular tumor antigens (54), a more diverse BCR repertoire will improve the chance of a successful antigen presentation. The strong association between patient survival after ICI and BCR diversity, but not clonality, further implies that ICI response depends on successful tumor antigen presentation to T cells and not on the subsequent clonal expansion and differentiation of B cells into long lived antibody producing plasma cells.

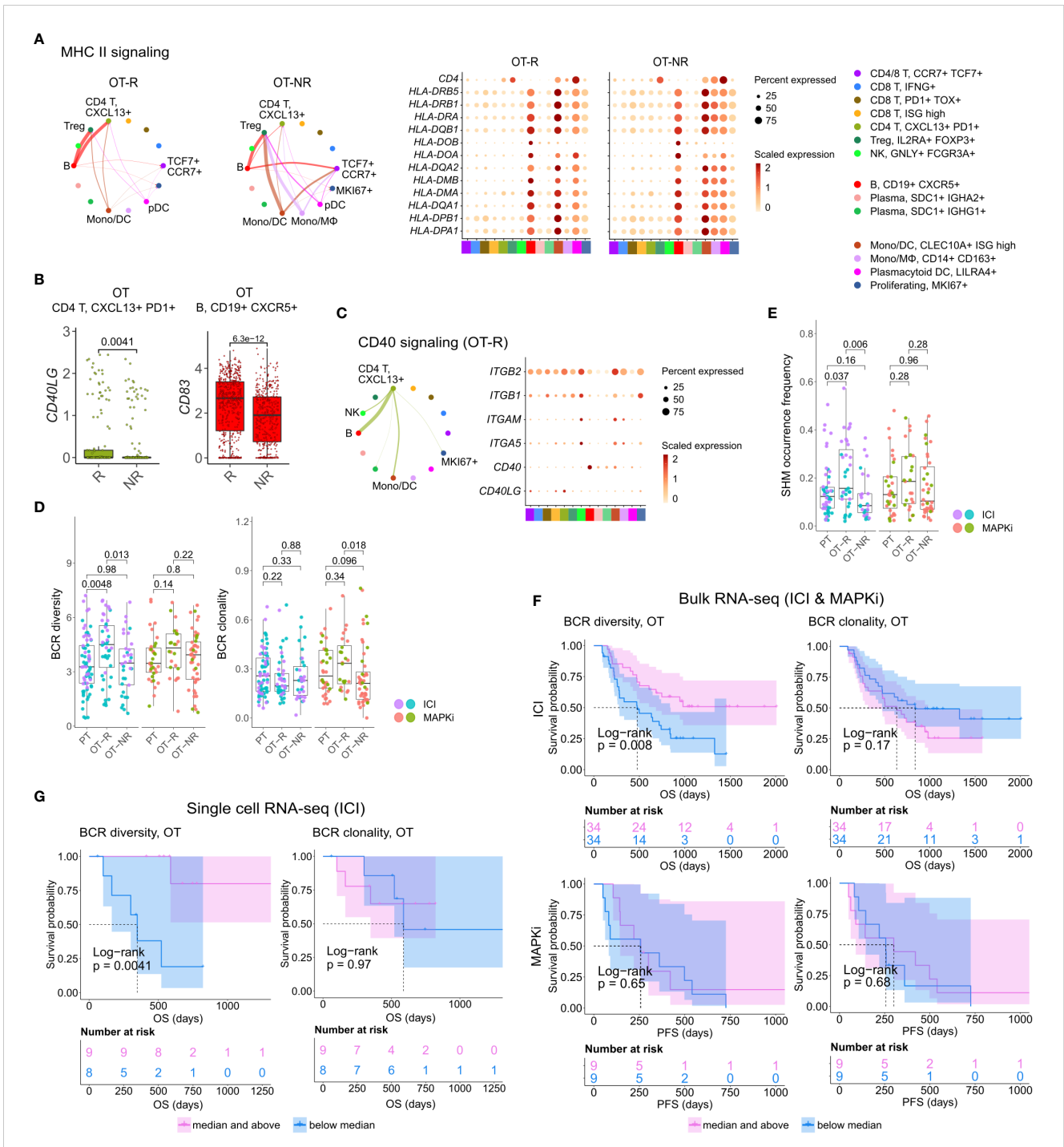


FIGURE 4
 B cells in ICI OT-R tumors present antigens to *PDCD1+ TOX+* tumor-reactive CD8 T and CD4 Tfh cells via the MHC I and II pathways. **(A)** Predicted enrichment of cell-to-cell interaction through MHC II antigen presentation pathway (left) and the normalized expression of MHC II-related genes (right). The expressions of MHC II genes are similar between ICI OT-R and OT-NR but, because of the higher proportion of B cells in ICI OT-R, the predicted MHC II interaction is (relatively) dominated by B cells in ICI OT-R. The interaction is more evenly distributed among the monocytic DCs, macrophages, and B cells in ICI OT-NR tumors. **(B)** Normalized expression of *CD40LG* and *CD83* in follicular helper T cell (Tfh) and CXCR5+ B cell populations, respectively. **(C)** Predicted enrichment of cell-to-cell interaction through CD40L/CD40 pathway specific to ICI OT-R tumors (left) and the normalized expression of CD40 pathway related genes (right). **(D)** BCR clonotype diversity and clonality among the PT, OT-R and OT-NR tumors in the ICI or MAPKi therapy group. The BCR clones are based on TRUST4's predicted CDR3 sequences of the immunoglobulin heavy (IGH) chains in each RNA-seq sample (see Methods). **(E)** Somatic hypermutation (SHM) frequencies based on predicted germline (i.e., prior to SHM) BCR clones by SCOPer (see Methods). **(F)** Kaplan-Meier survival curves of ICI- or MAPKi-treated melanoma patients in the bulk RNA-seq datasets stratified by either the BCR diversity (left) or clonality (right) of their OT tumors. **(G)** Kaplan-Meier survival curves of ICI-treated patients in the scRNA-seq dataset stratified by either the BCR diversity (left) or clonality (right) of their OT tumors.

Combined increase in BCR diversity and IFN γ pathway activity correlates with the greatest long-term survival after ICI therapy

Successful antigen recognition by CD8 T cells increased the overall IFN γ expression (Supp. Figure 5A), which subsequently induced IFN γ pathway activation in the TME of ICI OT-R tumors (Figure 1F). IFN γ expression by multiple CD8 T cell populations mostly activated the IFN γ pathway in B cells and monocytic DCs from ICI OT-R tumors (Figure 5A). The activation of IFN γ pathway in these immune populations is expected to boost their antigen presentation activity, resulting in additional Tfh and CD8 T cell activation. In OT-NR tumors, IFN γ pathway interaction mainly involved the immunosuppressive CD14+ CD163+ M ϕ and monocytic DCs (Figure 5A).

When stratified by the enrichment of hallmark interferon gamma gene set and BCR diversity of their tumors (high: median and above, and, low: below median), ICI-treated patients with the best survival were those with high hallmark interferon gamma gene set and BCR diversity in their OT samples (Figure 5B, log-rank $P=0.0072$). Cox proportional hazard analyses suggested that hallmark interferon gamma gene set score and BCR diversity in the OT samples are independent predictors of survival in ICI treated patients (Figure 5C; Supp. Table 4C). Stratification of the patients by the expression of CD8 T cell marker *CD8B* and B cell marker *CD19* show a similar trend where patients with high expression of both *CD19* and *CD8B* had better survival after ICI treatment (Supp. Figure 5B), which is in agreement with a recent report on a separate cohort of melanoma patients (29). Curiously, our analysis also revealed an interaction/dependency between BCR diversity and hallmark interferon gamma gene set scores in relation with the patients' OS (Supp. Figure 5C; Supp. Table 4D, HR of interaction = 0.55, $P = 0.054$). Indeed, the combined positive effect of clonally diverse B cells and high IFN γ signaling pathway activity (indicating successful antigen presentation to T cells) on patients' OS is significantly greater the sum of their individual effects (Figure 5B). Thus, higher clonal diversity of intratumoral B cells and IFN γ signaling pathway activity in the TME may act synergistically to drive a durable ICI response.

Discussion

To discover immune factors and pathways associated with durable response to ICI-based immunotherapy, we analyzed the transcriptomic profiles of melanoma biopsies taken before and after ICI treatment. Unique to our study is the use of transcriptomic profiles of melanoma biopsied pre- and post-MAPKi therapy. Since MAPKi therapy also induces significant immune infiltration, yet MAPKi-treated patients are less likely to achieve a durable response than ICI-treated patients, comparing immune infiltration associated with ICI against MAPKi allowed us to separate drivers of durable response from immune "bystanders" in ICI OT-R tumors. Genes that are upregulated in ICI OT-R tumors highlighted enrichment of B cell and Tfh gene markers, strongly

hinting the presence of TLS in the tumor. This observation confirms previous studies reporting positive association between TLS and ICI response in multiple cancer histologies (28–31).

In ICI OT-R tumors, the increase of TLS-associated CXCR5+ B and Tfh cells were correlated with increased mRNA expression of CXCR5's ligand, *CXCL13*, by activated, tumor reactive CXCL13+ CD8 T cells (50). We propose a model where an effective response to ICI is marked with CXCL13+ CD8 T cell-driven recruitment of highly diversified, CXCR5+ B cell clones whose subsequent (tumor) antigen presentation activities induce and sustain the activation of tumor-reactive CD4 Tfh and CD8 T cells (Figure 5D). Notably, our model resembles the cancer-immunity cycle initially proposed by Chen and Mellman (58) with the important distinctions of the cycle happening directly in the TME and CXCR5+ B cells functioning as its major APC.

Our cell-cell interaction analysis highlighted CXCR5+ B cells as the dominant antigen presenting cells in ICI OT-R TME, presenting antigens to both tumor-reactive CD8 T cells and CD4 Tfh cells and through MHC I and MHC II pathways, respectively. We observed a concomitant overexpression of *CD40LG* in the Tfh population, reflecting a productive antigen presentation by B cells to Tfh (53, 54). CD40L up-expression in Tfh then activated the CD40 signaling pathway in B cells, as shown by upregulation of *CD83* in the B cells (55). CD83 is a marker of light zone-specific, antigen presenting GC B cells (52) and its expression is crucial for B cell longevity after antigen stimulation (59). Overall upregulation of IFN γ expression in ICI OT-R tumors (bulk RNA-seq) was predicted to significantly activate the IFN γ pathway of B cells and DC in ICI OT-R tumors. Notably, simultaneous activation of IFN γ and CD40 signaling pathways in B cells can increase their antigen cross presentation to CD8 T cells (56, 60). Successful cross-presentation to tumor reactive CD8 T cells is expected to drive their cytotoxic activity against the tumor.

Another support of B cells' antigen presenting role in ICI response comes from the clonal dynamics of B cells in ICI OT-R tumors. Higher BCR diversity, which is expected to increase the chance of tumor antigen uptake and presentation to T cells, is significantly correlated with longer OS after ICI therapy both in the bulk and single-cell RNA-seq cohorts of melanoma patients. However, higher BCR clonality is not associated with improved OS after ICI. This suggests that B cells' subsequent clonal expansion and differentiation into long-lived plasma/memory B cells are less correlated with response to ICI than the diversity of their presented antigens. Finally, we demonstrated that BCR diversity and IFN γ signaling pathway scores are both significant and synergistic variables that are correlated with patient survival after ICI therapy.

Our study has several limitations. First, it is a correlative, retrospective study of combined cohorts of ICI-treated tumors. To overcome this, we ensured that the most important observations from one dataset are corroborated an independent dataset. For instance, the increased expression of TLS markers in ICI OT-R tumors and the association between BCR diversity/clonality with survival were confirmed in both bulk and scRNA-seq datasets of ICI treated melanoma. We also validated the differential effects of ICI (using a PD-1 antibody) and MAPKi on CXCL13 expression by activated T cells, albeit in an *in vitro* context. Another limitation is

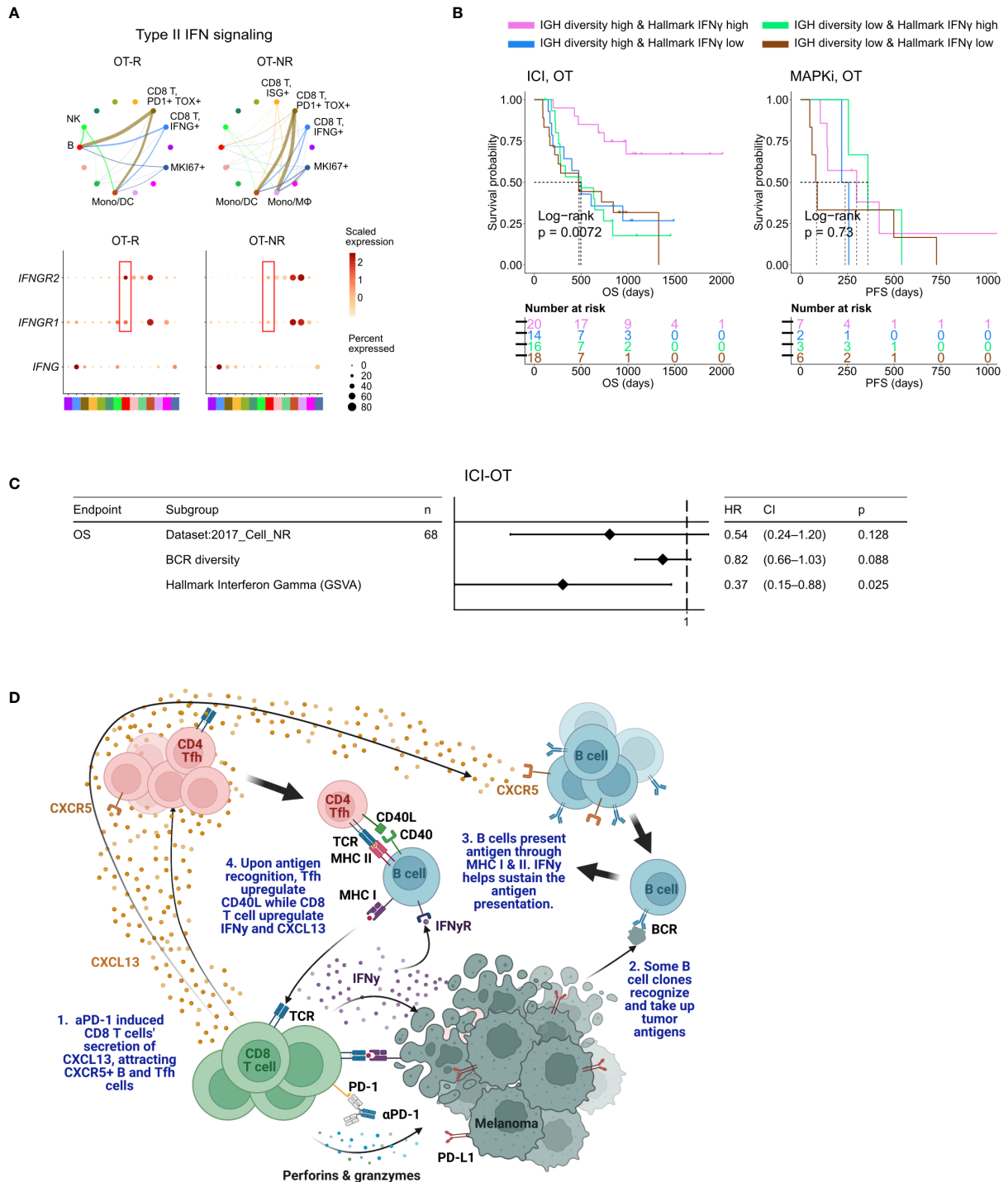


FIGURE 5

BCR diversity and IFN γ signaling pathway activation are significant factors associated with enhanced OS after ICI therapy. **(A)** Predicted enrichment of receptor–ligand interaction involving type II IFN signaling between *IFNG* expression CD8 T cell clusters and B cells in ICI OT-R tumors (top). Increased expression of *IFNGR1/2* in the B cells of ICI-responders (bottom) is expected to further enhance B cells’ antigen presentation activity. **(B)** Kaplan–Meier survival curves of patients stratified by BCR diversity and hallmark interferon gamma gene set score in OT tumors of the ICI or MAPKi therapy group. **(C)** Multivariate Cox proportional hazards analysis assessing the hazard ratios of BCR diversity and hallmark interferon gamma gene set score in ICI OT tumor samples. **(D)** The schematic of our proposed model of productive ICI response. First, tumor-reactive CD8 T cells produce CXCL13 in response to ICI to recruit TLS-associated CXCR5+ Tfh and B cells. B cells pick up tumor antigens from tumor cells debris, potentially killed by ICI-activated CD8 T cells. Successful tumor antigen presentation by B cells, expected to highly correlate with their BCR repertoire diversity, results in the activation of the Tfh and (additional) tumor reactive CD8 T cells. Tfh and CD8 T cells upregulate CD40L and IFN γ , respectively, resulting in enhancement of B cell antigen presentation activity. Finally, newly activated, tumor reactive CD8 T cells kill more tumor cells and secrete more CXCL13 to recruit additional CXCR5+ Tfh and B cells, thus completing an *in situ* cancer immunity cycle. Image created with BioRender.com.

that the use of RNA-seq to reconstruct the CDR3 regions of the TCR or BCR may have limited sensitivity. Additional studies using more samples in general and using direct TCR/BCR sequencing of ICI-treated tumors to measure T/B cell diversity and clonality are necessary to confirm our observations.

Our results demonstrate that an effective immune response to ICI involves activation of tumor reactive CD4 and CD8 T cells by antigen presenting B cells, in the context of TLS in the TME. Our finding is in line with a recent scRNA-seq study of ICI-treated triple negative breast cancer patients, which highlighted an enrichment of antigen presentation activity, rather than antibody production, in B cells of ICI-responding tumors (61). The next logical question is how to leverage this observation in the clinic. Several studies have attempted direct TLS formation using secreted factors such as CXCL13 (62). However, TLS formation may not be sufficient to ensure B cell and T cell activation and the subsequent antitumor immunity (63). Strategies to pre-load tumor antigens on B cells to generate B cell vaccine may be more promising as a combinatorial therapy with ICI. B cell-based tumor antigen vaccine was reported to promote ICI efficacy in animal models of melanoma (60), lung cancer (54) and glioblastoma (56). Thus, there is a pressing need for additional pre-clinical and, ultimately, clinical studies to test the most optimal B cell-vaccine approach that can enhance the rate of durable ICI response.

Data availability statement

The original contributions presented in the study are included in the article/Supplementary Material. All the source codes used in this study were uploaded to GitHub repository at https://github.com/sciencepeak/TCR_BCR_project. Further inquiries can be directed to the corresponding authors.

Ethics statement

Ethical review and approval was not required for the study on human participants in accordance with the local legislation and institutional requirements. Written informed consent for participation was not required for this study in accordance with the national legislation and the institutional requirements.

Author contributions

LD, LS, ML, and WH designed the experiments and analyses. LD implemented of the overall computational analyses unless specified otherwise. LS developed the single cell analysis pipeline. LD, LS, and MB performed single cell analysis. LNS and ML designed and performed the *in vitro* experiments. YZ contributed to this study as a visiting scientist at Division of Dermatology, Department of Medicine, UCLA. LD, RP, MS, ML, and WH wrote and edited the manuscript. All authors contributed to the article and approved the submitted version.

Funding

This study was funded in part by the NIH/NCI grant (1R01CA236910) and a grant from Parker Institute for Cancer Immunotherapy. LD is supported by grant from Parker Institute for Cancer Immunotherapy at UCLA and a postdoctoral fellowship from National Cancer Center. WH is supported by grants from NIH/NCI (1R01CA236910), the Jonnson Comprehensive Cancer Center, the Melanoma Research Alliance, the Margaret E. Early Medical Research Trust, and the Parker Institute for Cancer Immunotherapy at UCLA. ML is supported by grants from the NIH/NIDDK (K08DK129829) and the Aramont Charitable Foundation.

Acknowledgments

We thank Moshe Sade-Feldman and Nir Hacohen for generously providing the raw count expression data of single cell RNA-seq used in their publication.

Conflict of interest

The authors declare that the research was conducted in the absence of any commercial or financial relationships that could be construed as a potential conflict of interest.

The reviewer HS declared a shared affiliation with the authors to the handling editor at the time of review.

Publisher's note

All claims expressed in this article are solely those of the authors and do not necessarily represent those of their affiliated organizations, or those of the publisher, the editors and the reviewers. Any product that may be evaluated in this article, or claim that may be made by its manufacturer, is not guaranteed or endorsed by the publisher.

Supplementary material

The Supplementary Material for this article can be found online at: <https://www.frontiersin.org/articles/10.3389/fimmu.2023.1176994/full#supplementary-material>

SUPPLEMENTARY FIGURE 1

Shared and therapy-specific transcriptomic changes after ICI or MAPKi therapy. (A) Schematic of the bulk RNA-seq data sets of ICI- and MAPKi-treated melanoma used in this study. (B, C) Normalized expression of T cell marker genes (*CD3D*, *CD8B*) (B) and GSVA gene set enrichment scores of interferon gamma gene sets from the Molecular Signature database (C) in the PT, OT-R and OT-NR samples of patients treated with ICI or MAPKi therapy (inter therapy comparison). (D) Kaplan-Meier survival curves of ICI- or MAPKi-treated melanoma patients stratified by either *CD8B* expression (left) or hallmark interferon gamma response gene set scores (right) in their PT tumors. (E) Kaplan-Meier survival curves of overall (top) or progression free survival (bottom) of MAPKi-treated melanoma patients stratified by either *CD8B* expression (left) or hallmark interferon gamma response gene set scores

(right) in their OT tumors (two independent microarray datasets of MAPKi-treated melanoma patients). (F) Correlation between PFS and OS after MAPKi therapy across two separate melanoma microarray datasets. (G) Normalized expression of T cell cytotoxicity genes *GZMB* and *PRF1* in the PT, OT-R and OT-NR samples of patients treated with ICI or MAPKi therapy.

SUPPLEMENTARY FIGURE 2

Characterization of B cell and TLS-related gene expression changes after ICI and MAPKi therapy. (A) Enriched tissue specific gene sets in DEGs upregulated in MAPKi OT-R tumors with respect to ICI OT-R tumors (after adjustment by respective therapy group's OT-NR tumors). (B) Normalized expression of the listed B cell-related genes among the PT, OT-R and OT-NR tumors in the ICI or MAPKi therapy group. (C) Enrichment scores of a recently published TLS 7-gene and 9-gene gene sets among the PT, OT-R and OT-NR tumors in the ICI or MAPKi therapy group. (D) Kaplan-Meier survival curves of overall (top) or progression free survival (bottom) of MAPKi-treated melanoma patients stratified by either *CD19* expression (left) or TLS gene set enrichment score (right) in their OT tumors. (E) Kaplan-Meier survival curves of ICI- or MAPKi-treated melanoma patients stratified by either *CD19* expression (left) or TLS gene set enrichment score (right) in their PT tumors.

SUPPLEMENTARY FIGURE 3

Single cell analysis of ICI-treated melanoma. (A) The fraction of the myeloid and proliferating cell populations in stratified by response vs. non-response to ICI in PT (top) and OT tumors (bottom). (B) Kaplan-Meier survival curves of ICI-treated patients stratified by the proportion of monocyte/macrophages within either their PT (left) or OT tumors (right). (C) Single cell-based gene set enrichment score of the TLS 7-gene and 9-gene signatures projected on the UMAP (left) or presented in boxplot across all cell types (right). The scores were separated into quartiles to assist the visualization of high and low gene set enrichments in different cell populations.

SUPPLEMENTARY FIGURE 4

B cell-associated antigen presentation and clonotype analyses. (A) Inferred cell-cell communication among intratumoral immune populations of pre- and post-ICI treated melanoma across curated signaling pathways in CellChat. The interactions are grouped based on response vs. no-response to ICI in either PT or OT tumors. (B) Predicted enrichment of cell-to-cell interaction through MHC I antigen presentation pathway. (C, D) Change in BCR (C) or TCR (D) clonal fraction in grouped by clones found only in the OT sample (OT-specific), only in the PT (PT-specific) and both in the PT and OT samples (overlapping, see illustration on the left). These fractions are calculated with respect to the union of all BCR/TCR clones found in the PT and OT samples of each patient; this analysis is done only on patients with PT and OT tumors.

SUPPLEMENTARY FIGURE 5

Multivariate analysis of survival examining the association among T cell and B cell related variables to patient OS after ICI therapy. (A) Normalized bulk RNA-seq expression of *IFNG* in the PT, OT-R and OT-NR samples of patients treated with ICI or MAPKi therapy. (B) Kaplan-Meier survival curves of patients stratified by normalized expressions of *CD8B* and *CD19* in either PT or OT tumors of the ICI or MAPKi therapy group. (C) Multivariate Cox proportional hazards analysis assessing the hazard ratios of BCR diversity, hallmark interferon gamma gene set score, and their interaction in ICI OT tumor samples.

SUPPLEMENTARY TABLE 1

Clinical characteristics, gene expression and gene set enrichments in the bulk RNA-seq datasets. (A) Summary of clinical data associated with the tumor samples (bulk and scRNA-seq datasets). (B) Difference in fold changes of OT-R vs. OT-NR samples after ICI or MAPKi therapy. (C) Gene sets/cell markers enriched in tumors responding to ICI, MAPKi or both (Enrichr analysis). (D) The relative abundance of immune and stromal cell populations in each sample in bulk RNA-seq dataset (MCPcounter analysis). (E) GSVA score matrix of selected gene sets of the bulk RNA-seq data of ICI or MAPKi-treated tumors.

SUPPLEMENTARY TABLE 2

PFS and OS correlation in MAPKi-treated melanoma patients. (A) OS and PFS data from two MAPKi treated gene expression microarray datasets (Rizos et al CCR 2014 and Long et al Nat. Comm. 2014).

SUPPLEMENTARY TABLE 3

Cell type fraction, DEGs and survival analysis of scRNA-seq data set of ICI-treated melanoma. (A) Differentially upregulated genes in each single cell cluster of CD45+ cells from ICI-treated tumors. (B) The fraction of immune cell populations in each PT/OT tumor sample of ICI-treated melanoma patients. (C) The association between the fraction each immune population (in PT or OT tumors) and OS after ICI therapy. (D) Differentially expressed genes in PT and OT tumors based on response (R) vs. no-response (NR) to ICI. (E) The association between TCR/BCR clonality or diversity in PT or OT tumors and OS after ICI therapy.

SUPPLEMENTARY TABLE 4

Univariate and multivariate survival analyses of B cell, T cell and TLS-related gene/gene sets. (A) TCR and BCR clonotype repertoire metrics of the ICI and MAPKi datasets (bulk and scRNA-seq). (B) Univariate CoxPH analysis of survival of B cell, T cell and TLS-related gene/gene sets (bulk RNA-seq cohorts). (C) Multivariate CoxPH analysis of survival of significant B cell, T cell and TLS-related gene/gene sets (ICI-OT only, pairwise independent). (D) Multivariate CoxPH analysis of survival of significant B cell, T cell and TLS-related gene/gene sets (ICI-OT only, with pairwise interaction term).

References

- Luke JJ, Schwartz GK. Chemotherapy in the management of advanced cutaneous malignant melanoma. *Clinics Dermatol* (2013) 31:290–7. doi: 10.1016/j.clindermatol.2012.08.016
- Luke JJ, Flaherty KT, Ribas A, Long GV. Targeted agents and immunotherapies: optimizing outcomes in melanoma. *Nat Rev Clin Oncol* (2017) 14:463–82. doi: 10.1038/nrclinonc.2017.43
- Curti BD, Faries MB. Recent advances in the treatment of melanoma. *New Engl J Med* (2021) 384:2229–40. doi: 10.1056/NEJMra2034861
- Tawbi HA, Schadendorf D, Lipson EJ, Ascierto PA, Matamala L, Castillo Gutierrez E, et al. Relatlimab and nivolumab versus nivolumab in untreated advanced melanoma. *New Engl J Med* (2022) 386:24–34. doi: 10.1056/NEJMoa2109970
- Hodi FS, O'Day SJ, McDermott DF, Weber RW, Sosman JA, Haanen JB, et al. Improved survival with ipilimumab in patients with metastatic melanoma. *New Engl J Med* (2010) 363:711–23. doi: 10.1056/NEJMoa1003466
- Robert C, Schachter J, Long GV, Arance A, Grob JJ, Mortier L, et al. Pembrolizumab versus ipilimumab in advanced melanoma. *New Engl J Med* (2015) 372:2521–32. doi: 10.1056/NEJMoa1503093
- Robert C, Long GV, Brady B, Dutriaux C, Maio M, Mortier L, et al. Nivolumab in previously untreated melanoma without BRAF mutation. *New Engl J Med* (2014) 372:320–30. doi: 10.1056/NEJMoa1412082
- Larkin J, Chiarion-Sileni V, Gonzalez R, Grob JJ, Cowey CL, Lao CD, et al. Combined nivolumab and ipilimumab or monotherapy in untreated melanoma. *New Engl J Med* (2015) 373:23–34. doi: 10.1056/NEJMoa1504030
- Kalbasi A, Ribas A. Tumour-intrinsic resistance to immune checkpoint blockade. *Nat Rev Immunol* (2020) 20:25–39. doi: 10.1038/s41577-019-0218-4
- Schoenfeld AJ, Hellmann MD. Acquired resistance to immune checkpoint inhibitors. *Cancer Cell* (2020) 37:443–55. doi: 10.1016/j.ccell.2020.03.017
- Nowicki TS, Hu-Lieskovan S, Ribas A. Mechanisms of resistance to PD-1 and PD-L1 blockade. *Cancer J* (2018) 24:47–53. doi: 10.1097/PPO.0000000000000303
- Bruni D, Angell HK, Galon J. The immune contexture and immunoscore in cancer prognosis and therapeutic efficacy. *Nat Rev Cancer* (2020) 20:662–80. doi: 10.1038/s41568-020-0285-7
- Tumeh PC, Harview CL, Yearley JH, Shintaku IP, Taylor EJM, Robert L, et al. PD-1 blockade induces responses by inhibiting adaptive immune resistance. *Nature* (2014) 515:568–71. doi: 10.1038/nature13954
- Ayers M, Lunceford J, Nebozhyn M, Murphy E, Loboda A, Kaufman DR, et al. IFN- γ -related mRNA profile predicts clinical response to PD-1 blockade. *J Clin Invest* (2017) 127:2930–40. doi: 10.1172/JCI91190
- Chen P-L, Roh W, Reuben A, Cooper ZA, Spencer CN, Prieto PA, et al. Analysis of immune signatures in longitudinal tumor samples yields insight into biomarkers of response and mechanisms of resistance to immune checkpoint blockade. *Cancer Discovery* (2016) 6:827–37. doi: 10.1158/2159-8290.CD-15-1545
- Abril-Rodriguez G, Torrejon DY, Liu W, Zaretsky JM, Nowicki TS, Tsoi J, et al. PAK4 inhibition improves PD-1 blockade immunotherapy. *Nat Cancer* (2020) 1:46–58. doi: 10.1038/s43018-019-0003-0
- Grasso CS, Tsoi J, Onyshchenko M, Abril-Rodriguez G, Ross-Macdonald P, Wind-Rotolo M, et al. Conserved interferon- γ signaling drives clinical response to immune checkpoint blockade therapy in melanoma. *Cancer Cell* (2020) 38:500–15.e3. doi: 10.1016/j.ccell.2020.08.005

18. Davies H, Bignell GR, Cox C, Stephens P, Edkins S, Clegg S, et al. Mutations of the BRAF gene in human cancer. *Nature* (2002) 417:949–54. doi: 10.1038/nature00766
19. Long GV, Stroyakovskiy D, Gogas H, Levchenko E, de Braud F, Larkin J, et al. Combined BRAF and MEK inhibition versus BRAF inhibition alone in melanoma. *New Engl J Med* (2014) 371:1877–88. doi: 10.1056/NEJMoa1406037
20. Larkin J, Ascierto PA, Drèno B, Atkinson V, Liskay G, Maio M, et al. Combined vemurafenib and cobimetinib in BRAF-mutated melanoma. *New Engl J Med* (2014) 371:1867–76. doi: 10.1056/NEJMoa1408868
21. Dummer R, Ascierto PA, Gogas HJ, Arance A, Mandala M, Liskay G, et al. Encorafenib plus binimetinib versus vemurafenib or encorafenib in patients with BRAF-mutant melanoma (COLUMBUS): a multicentre, open-label, randomised phase 3 trial. *Lancet Oncol* (2018) 19:603–15. doi: 10.1016/S1470-2045(18)30142-6
22. Knight DA, Ngiew SF, Li M, Parmenter T, Mok S, Cass A, et al. Host immunity contributes to the anti-melanoma activity of BRAF inhibitors. *J Clin Invest* (2013) 123:1371–81. doi: 10.1172/JCI66236
23. Song C, Piva M, Sun L, Hong A, Moriceau G, Kong X, et al. Recurrent tumor cell-intrinsic and -extrinsic alterations during MAPKi-induced melanoma regression and early adaptation. *Cancer Discov* (2017) 7:1248–65. doi: 10.1158/2159-8290.CD-17-0401
24. Robert C, Grob JJ, Stroyakovskiy D, Karaszewska B, Hauschild A, Levchenko E, et al. Five-year outcomes with dabrafenib plus trametinib in metastatic melanoma. *New Engl J Med* (2019) 381:626–36. doi: 10.1056/NEJMoa1904059
25. Ascierto PA, Drèno B, Larkin J, Ribas A, Liskay G, Maio M, et al. 5-year outcomes with cobimetinib plus vemurafenib in BRAFV600 mutation-positive advanced melanoma: extended follow-up of the coBRIM study. *Clin Cancer Res* (2021) 27:5225–35. doi: 10.1158/1078-0432.CCR-21-0809
26. Larkin J, Chiarion-Sileni V, Gonzalez R, Grob JJ, Rutkowski P, Lao CD, et al. Five-year survival with combined nivolumab and ipilimumab in advanced melanoma. *N Engl J Med* (2019) 381:1535–46. doi: 10.1056/NEJMoa1910836
27. Atkins MB, Tarhini A, Rael M, Gupte-Singh K, O'Brien E, Ritchings C, et al. Comparative efficacy of combination immunotherapy and targeted therapy in the treatment of BRAF-mutant advanced melanoma: a matching-adjusted indirect comparison. *Immunotherapy* (2019) 11:617–29. doi: 10.2217/imt-2018-0208
28. Helmink BA, Reddy SM, Gao J, Zhang S, Basar R, Thakur R, et al. B cells and tertiary lymphoid structures promote immunotherapy response. *Nature* (2020) 577:549–55. doi: 10.1038/s41586-019-1922-8
29. Cabrita R, Lauss M, Sanna A, Donia M, Skaarup Larsen M, Mitra S, et al. Tertiary lymphoid structures improve immunotherapy and survival in melanoma. *Nature* (2020) 577:561–5. doi: 10.1038/s41586-019-1914-8
30. Petitprez F, de Reyniès A, Keung EZ, Chen TW-W, Sun C-M, Calderaro J, et al. B cells are associated with survival and immunotherapy response in sarcoma. *Nature* (2020) 577:556–60. doi: 10.1038/s41586-019-1906-8
31. Meylan M, Petitprez F, Becht E, Bougouin A, Pupier G, Calvez A, et al. Tertiary lymphoid structures generate and propagate anti-tumor antibody-producing plasma cells in renal cell cancer. *Immunity* (2022) 55:527–41.e5. doi: 10.1016/j.immuni.2022.02.001
32. Riaz N, Havel JJ, Makarov V, Desrichard A, Urba WJ, Sims JS, et al. Tumor and microenvironment evolution during immunotherapy with nivolumab. *Cell* (2017) 171:934–49.e16. doi: 10.1016/j.cell.2017.09.028
33. Hugo W, Shi H, Sun L, Piva M, Song C, Kong X, et al. Non-genomic and immune evolution of melanoma acquiring MAPKi resistance. *Cell* (2015) 162:1271–85. doi: 10.1016/j.cell.2015.07.061
34. Kwong LN, Boland GM, Frederick DT, Helms TL, Akid AT, Miller JP, et al. Co-Clinical assessment identifies patterns of BRAF inhibitor resistance in melanoma. *J Clin Invest* (2015) 125:1459–70. doi: 10.1172/JCI78954
35. Rizos H, Menzies AM, Pupo GM, Carlino MS, Fung C, Hyman J, et al. BRAF inhibitor resistance mechanisms in metastatic melanoma: spectrum and clinical impact. *Clin Cancer Res* (2014) 20:1965–77. doi: 10.1158/1078-0432.CCR-13-3122
36. Long GV, Fung C, Menzies AM, Pupo GM, Carlino MS, Hyman J, et al. Increased MAPK reactivation in early resistance to dabrafenib/trametinib combination therapy of BRAF-mutant metastatic melanoma. *Nat Commun* (2014) 5:5694. doi: 10.1038/ncomms6694
37. Sade-Feldman M, Yizhak K, Bjorgaard SL, Ray JP, de Boer CG, Jenkins RW, et al. Defining T cell states associated with response to checkpoint immunotherapy in melanoma. *Cell* (2018) 175:998–1013.e20. doi: 10.1016/j.cell.2018.10.038
38. Kuleshov MV, Jones MR, Rouillard AD, Fernandez NF, Duan Q, Wang Z, et al. Enrichr: a comprehensive gene set enrichment analysis web server 2016 update. *Nucleic Acids Res* (2016) 44:W90–7. doi: 10.1093/nar/gkw377
39. Hänzelmann S, Castelo R, Guinney J. GSEA: gene set variation analysis for microarray and RNA-seq data. *BMC Bioinf* (2013) 14:7. doi: 10.1186/1471-2105-14-7
40. Subramanian A, Tamayo P, Mootha VK, Mukherjee S, Ebert BL, Gillette MA, et al. Gene set enrichment analysis: a knowledge-based approach for interpreting genome-wide expression profiles. *Proc Natl Acad Sci* (2005) 102:15545–50. doi: 10.1073/pnas.0506580102
41. Liberzon A, Birger C, Thorvaldsdóttir H, Ghandi M, Mesirov Jill P, Tamayo P. The molecular signatures database hallmark gene set collection. *Cell Syst* (2015) 1:417–25. doi: 10.1016/j.cels.2015.12.004
42. Song L, Cohen D, Ouyang Z, Cao Y, Hu X, Liu XS. TRUST4: immune repertoire reconstruction from bulk and single-cell RNA-seq data. *Nat Methods* (2021) 18:627–30. doi: 10.1038/s41592-021-01142-2
43. Nouri N, Kleinstein SH. Somatic hypermutation analysis for improved identification of b cell clonal families from next-generation sequencing data. *PLoS Comput Biol* (2020) 16:e1007977. doi: 10.1371/journal.pcbi.1007977
44. De Silva NS, Klein U. Dynamics of b cells in germinal centres. *Nat Rev Immunol* (2015) 15:137–48. doi: 10.1038/nri3804
45. Gupta NT, Vander Heiden JA, Uduman M, Gadala-Maria D, Yaari G, Kleinstein SH. Change-O: a toolkit for analyzing large-scale b cell immunoglobulin repertoire sequencing data. *Bioinformatics* (2015) 31:3356–8. doi: 10.1093/bioinformatics/btv359
46. Flaherty KT, Infante JR, Daud A, Gonzalez R, Kefford RF, Sosman J, et al. Combined BRAF and MEK inhibition in melanoma with BRAF V600 mutations. *N Engl J Med* (2012) 367:1694–703. doi: 10.1056/NEJMoa1210093
47. Freshwater T, Kondic A, Ahamadi M, Li CH, de Greef R, de Alwis D, et al. Evaluation of dosing strategy for pembrolizumab for oncology indications. *J Immunother Cancer* (2017) 5:43. doi: 10.1186/s40425-017-0242-5
48. Hong A, Piva M, Liu S, Hugo W, Lomeli SH, Zoete V, et al. Durable suppression of acquired MEK inhibitor resistance in cancer by sequestering MEK from ERK and promoting antitumor T-cell immunity. *Cancer Discovery* (2021) 11:714–35. doi: 10.1158/2159-8290.CD-20-0873
49. Beltra J-C, Manne S, Abdel-Hakeem MS, Kurachi M, Giles JR, Chen Z, et al. Developmental relationships of four exhausted CD8+ T cell subsets reveals underlying transcriptional and epigenetic landscape control mechanisms. *Immunity* (2020) 52:825–41.e8. doi: 10.1016/j.immuni.2020.04.014
50. Lowery FJ, Krishna S, Yossef R, Parikh NB, Chatani PD, Zacharakis N, et al. Molecular signatures of antitumor neoantigen-reactive T cells from metastatic human cancers. *Science* (2022) 375:877–84. doi: 10.1126/science.abl5447
51. Aibar S, González-Blas CB, Moerman T, Huynh-Thu VA, Imrichova H, Hulselman G, et al. SCENIC: single-cell regulatory network inference and clustering. *Nat Methods* (2017) 14:1083–6. doi: 10.1038/nmeth.4463
52. Cyster JG, Allen CDC. B cell responses: cell interaction dynamics and decisions. *Cell* (2019) 177:524–40. doi: 10.1016/j.cell.2019.03.016
53. Crotty S. T Follicular helper cell biology: a decade of discovery and diseases. *Immunity* (2019) 50:1132–48. doi: 10.1016/j.immuni.2019.04.011
54. Cui C, Wang J, Fagerberg E, Chen P-M, Connolly KA, Damo M, et al. Neoantigen-driven b cell and CD4 T follicular helper cell collaboration promotes anti-tumor CD8 T cell responses. *Cell* (2021) 184:6101–18.e13. doi: 10.1016/j.cell.2021.11.007
55. Kretschmer B, Kuhl S, Fleischer B, Breloer M. Activated T cells induce rapid CD83 expression on b cells by engagement of CD40. *Immunol Lett* (2011) 136:221–7. doi: 10.1016/j.imlet.2011.01.013
56. Lee-Chang C, Miska J, Hou D, Rashidi A, Zhang P, Burga RA, et al. Activation of 4-1BBL+ b cells with CD40 agonism and IFN γ elicits potent immunity against glioblastoma. *J Exp Med* (2020) 218(1):e20200913. doi: 10.1084/jem.20200913
57. Yost KE, Satpathy AT, Wells DK, Qi Y, Wang C, Kageyama R, et al. Clonal replacement of tumor-specific T cells following PD-1 blockade. *Nat Med* (2019) 25:1251–9. doi: 10.1038/s41591-019-0522-3
58. Chen DS, Mellman I. Oncology meets immunology: the cancer-immunity cycle. *Immunity* (2013) 39:1–10. doi: 10.1016/j.immuni.2013.07.012
59. Prazma CM, Yazawa N, Fujimoto Y, Fujimoto M, Tedder TF. CD83 expression is a sensitive marker of activation required for b cell and CD4+ T cell longevity in vivo. *J Immunol* (2007) 179:4550–62. doi: 10.4049/jimmunol.179.7.4550
60. Wennhold K, Weber TM, Klein-Gonzalez N, Thelen M, Garcia-Marquez M, Chakupurakal G, et al. CD40-activated b cells induce anti-tumor immunity in vivo. *Oncotarget* (2017) 8:27740–53. doi: 10.18632/oncotarget.7720
61. Zhang Y, Chen H, Mo H, Hu X, Gao R, Zhao Y, et al. Single-cell analyses reveal key immune cell subsets associated with response to PD-L1 blockade in triple-negative breast cancer. *Cancer Cell* (2021) 39:1578–93 e8. doi: 10.1016/j.ccell.2021.09.010
62. Ukita M, Hamanishi J, Yoshitomi H, Yamanoi K, Takamatsu S, Ueda A, et al. CXCL13-producing CD4+ T cells accumulate in the early phase of tertiary lymphoid structures in ovarian cancer. *JCI Insight* (2022) 7(12):e157215. doi: 10.1172/jci.insight.157215
63. van Hooren L, Vaccaro A, Ramachandran M, Vazaios K, Libard S, van de Walle T, et al. Agonistic CD40 therapy induces tertiary lymphoid structures but impairs responses to checkpoint blockade in glioma. *Nat Commun* (2021) 12:4127. doi: 10.1038/s41467-021-24347-7